AD-449958

ONR Contract No. Nonr 591-(10)
R.P.I. Project No. 441.35

Technical Report No.23
October, 1964

The Thermodynamics of Corrosion in Molten Carbonates: Application of E-pCO_2 Diagrams

by

M.D. Ingram and G.J. Janz

Department of Chemistry
Rensselaer Polytechnic Institute
Troy, New York

To be published in J. Electrochemical Society

The Thermodynamics of Corrosion in Molten Carbonates: Application of E-pCO_2 Diagrams

by

Malcolm D. Ingram and George J. Janz

Rensselaer Polytechnic Institute, Department of Chemistry, Troy, New York

ABSTRACT

The corrosion of metals in fused carbonates is discussed in terms of a diagrammatic presentation of the thermodynamic data. The treatment closely resembles that of Pourbaix and Littlewood; diagrams are plotted of E versus pCO_2, where E is the redox potential of the system, and $pCO_2 = -\log_{10}(CO_2)$. Each diagram is divided into three regions which mark the limits of stability at unit activity of the pure metal, metal oxide, and liquid metal carbonate. In the oxide region the metal may become passivated, but this depends on structural factors and requires experimental confirmation. The electrochemical series in molten carbonates is presented, and the significance of pCO_2 in relation to acid-base behavior is discussed.

INTRODUCTION

Recent studies[1,2,3,4] have revealed a marked diversity in corrosion behavior when metal substrates are exposed to carbonate melts. Thus gold shows a high degree of nobility which does not depend on the formation of oxide film. On other metals oxide formation is common, and in the case of certain stainless steels this leads to passivation. However, despite the appearance of nickel oxide, attack on nickel proceeds with severity. An attempt to interpret these phenomena and to devise means of controlling corrosion must begin with a consideration of the thermodynamics of the metal fused-salt systems.

Pourbaix[5] has treated extensively corrosion in aqueous solutions, constructing diagrams in which the redox potential (E) is plotted versus pH. Littlewood[6] extended this approach to fused chlorides with similar plots of E versus $pO^{=}$. The diagrams were drawn up on the principle that, at equilibrium, the positions of all the redox potentials in a system may be expressed by a single potential. The advantage of this presentation is that the different factors which influence metal ionization and oxide formation may be compared at a glance.

In extending this treatment to molten carbonates it has been necessary to find a function, analogous to pH, which will express the acidity of the system. It is known that the dissociation of the carbonate anion gives rise to well defined acid-base behavior:

$$CO_3^{=} \rightleftharpoons O^{=} + CO_2$$

In terms of the Lux-Flood[7,8] concept, the $CO_3^{=}$ ion acts as a base in the supply of oxide ions, and carbon dioxide is its conjugate acid. It is apparent that the oxide activity does not take up an arbitrary value but varies continuously from zero to unity, depending on the pressure of carbon dioxide. The acidity of the melt, therefore, may be expressed either as $pO^{=}$ or as pCO_2 which are similarly defined: $pO^{=} = -\log_{10}(O^{=})$, $pCO_2 = -\log_{10}(CO_2)$. The latter function seems to have the greater practical usefulness since the pressure of carbon dioxide is usually fixed by the experimental conditions.

This communication reports the construction of E_{redox}-pCO_2 diagrams for a number of metals in a ternary eutectic of the alkali carbonates (Li:Na:K = 43.5:31.5:25.0.m.p = 397°C) at 600°C.

CONSTRUCTION OF THE DIAGRAMS

Sources of Thermodynamic Data

The first requirement in the construction of the diagrams is a set of self consistent thermal data. Accordingly, values were taken when possible from the critical compilations of the U. S. Bureau of Mines[9,10]. Estimated data were in some cases taken from JANAF[11] Tables. When published data were insufficient, extrapolations were made using the methods of Kubaschewski and Evans[12].

Sign Conventions

It is desirable to establish a potential scale in molten carbonates which is strictly analogous to that in aqueous systems. Standard potentials have therefore been calculated from the equation $\Delta G^{\circ} = -nE^{\circ}F$, Potentials defined in this way are in accord with the Stockholm Convention and express the polarity of the cell relative to the external circuit. Thus metal nobility is associated with a positive standard potential; similarly, a positive redox potential expresses oxidizing conditions in the melt.

Equilibria in the Carbonate Melt

The redox potential in the melt will depend on the pressures of

carbon dioxide and oxygen in the gas phase. Thus the oxidation of the carbonate ion may be written

$$CO_3^{=} - 2e^{-} \longrightarrow CO_2 + {}^{1}/_{2}O_2$$

Hence, if the $CO_3^{=}$ activity is close to unity,

$$E_{redox} = E^{0} - \frac{2.3RT}{2F} pCO_2 + \frac{2.3RT}{4F} \log_{10}(O_2) \qquad (1)$$

Experiments on the 'oxygen' electrode in carbonate melts have shown that Eq. (1) is accurately obeyed[13,14]. It provides a convenient reference scale of potential, E being set equal to zero for the most 'noble' mixture of CO_2 and O_2 at one atmosphere total pressure; i.e., when $CO_2:O_2 = 2:1$. Substituting in the appropriate values, one has at 600°C:

$$E_{redox} = 0.0359 + 0.086\ pCO_2 - 0.0433 \log_{10}(O_2) \qquad (1a)$$

Fig. (1) is the diagrammatic representation of Eq. (1a). The dependence of E_{redox} on pCO_2 is plotted; each line corresponds to a different partial pressure of oxygen, the values of $\log(O_2)$ being plotted on the outer framework. Thus, if the pressures of carbon dioxide and oxygen are known, the properties of the system may be defined uniquely by a point on the diagram.

If the dissociation of the carbonate ion is considered as:

$$M_2CO_3(liq) \rightleftharpoons M_2O(liq) + CO_2$$

then

$$\log_{10} K_d = \log_{10} \frac{(M_2O)(CO_2)}{(M_2CO_3)} \qquad (2)$$

Hence, if $(M_2CO_3) = 1$, and the melt is completely ionic,

$$pO^{=} + pCO_2 = -\log_{10} K_d \qquad (3)$$

Accurate calculation of K_d for the ternary eutectic is a difficult problem, which however may be simplified by using the Broers[15] treatment. It is assumed that the heat of mixing of the three carbonates is zero, and similarly for the three oxides. Since entropies of mixing will cancel in the reaction, the free energies of dissociation in the single salt melts will be additive in the mixture. Thus, at 600°C:

$$\log_{10} K_d = -11$$

and

$$pO^{=} = -11 + pCO_2 \qquad (3a)$$

This is the origin of the $pO^{=}$ scale at the top of the diagram, which, unlike the pCO_2 scale, will reflect the properties of the cations in the melt.

The range of values included on the axes is large: i.e., pCO_2 from +20 to -10, and $\log(O_2)$ from +40 to -80. However, the melt itself imposes certain limits on gas phase conditions with which it can equilibrate. For instance, inspection of the diagram shows that when $pCO_2 = +11$, $pO^{=} = 0$. This is clearly inconsistent with the assumption in Eq. (3)

that carbonate ion is at unit activity, and the treatment breaks down. Referring to Eq. (2) one finds that when $pCO_2 = -\log k_d \cdot (CO_3^{=}) = (O^{=})$, and this is in effect the 'basic' limit of the carbonate melt.

There is also a lower limit of electroactivity in the electrolyte. This may arise in several ways, including the decomposition of the melt:

$$M_2CO_3 \rightarrow 2M + CO_2 + \tfrac{1}{2}O_2$$

The appearance of alkali metal at unit activity will 'buffer' the redox potential at

$$E_{redox} = E^0_{M/M^+} + 2.3\frac{RT}{F} \log_{10}\frac{(M^+)}{1} \qquad (4)$$

In practice a liquid alloy of the three alkali metals will separate from the melt in equilibrium with each cation. If for simplicity the melt is treated as pure sodium carbonate (hypothetical liquid), the lower limit of electroactivity is a horizontal line at the standard potential of sodium. For the reaction:

$$Na_2CO_3\ (liq) \rightarrow 2Na(liq) + CO_2(2/3\ atm) + \tfrac{1}{2}O_2(1/3\ atm)$$

$$\Delta G = +\ 112 \quad k.cal.$$

Hence $$E^0_{Na/Na^+} = -\ 2.43\ v \qquad (5)$$

Alternatively, the decomposition of the melt could be forestalled by the reduction of carbon dioxide with the deposition of graphite, thus:

cathodic process: $3CO_2 + 4e^- \rightarrow 2CO_3^{=} + C$

anodic process: $2CO_3^{=} - 4e^- \rightarrow 2CO_2 + O_2$

overall process: $CO_2 \rightarrow C + O_2$

It follows from Eq. (14) that when graphite is present the potential is controlled by the carbon dioxide pressure, thus

$$E = E^{\circ} - \frac{3}{4} \cdot \frac{2.3RT}{F} pCO_2 \qquad (6)$$

$$= -1.011 - 0.130\ pCO_2 \qquad (6a)$$

Eq. (6a) gives rise to the sloping line in Fig. 1. It is clear that under normal conditions the appearance of graphite is thermodynamically preferred before alkali metal; however, the situation experimentally is not clear. In subsequent diagrams the limits to the melt performance are set by the lines: $E = -2.43V$, $pCO_2 = +11$.

Metal-Carbonate Equilibria

The E-pCO_2 grid provides a suitable framework for the electrochemical behavior of the different metals. Fig. 2 is the nickel diagram and its construction exemplifies the general treatment. It is divided into three regions in which only one nickel phase may be present at unit activity, viz. Ni metal, Ni^{2+}, and solid NiO.

In the Ni domain, the Ni^{2+} activity will depend only on the redox

potential and on the standard potential of nickel. Consider the formation cell

$$Ni \mid NiCO_3(liq) \mid CO_2(2/3\ atm).\ O_2(1/3\ atm)$$

For the cell reaction

$$NiCO_3 \rightarrow Ni + CO_2 + {}^1/_2O_2, \quad \Delta G = +15.72\ Kcal$$

Hence $$E^o_{Ni/Ni^{2+}} = -0.34V$$

and $$E_{redox} = -0.34 + 2.3\frac{RT}{ZF} \log(Ni^{2+}) \qquad (7)$$

In this way the (Ni^{2+}) scale has been included, which generates a series of isoactivity lines perpendicular to the E-axis.

Above its standard potential nickel cannot be in equilibrium with a carbonate melt. In this Ni^{2+} domain, Ni^{2+} ions may be present at activities ranging from zero to unity, since the redox potential governs only the ratio (Ni^{2+}/Ni).

The boundary between the Ni^{2+} and NiO areas is the value of pCO_2 when NiO precipitates from a pure nickel carbonate melt. As the NiO domain is crossed and the basicity of the system is increased, the equilibrium activity of Ni^{2+} in the melt decreases. For the reaction

$$NiCO_3(liq) \rightarrow NiO(s) + CO_2, \quad \Delta G = -20.93\ Kcals$$

Hence $K_d = \frac{(NiO)(CO_2)}{(NiCO_3)} = 10^{5.24}$

and $\log(Ni^{2+}) = -\log K_d - pCO_2$ (8)

$= -5.24 - pCO_2$ (8a)

The $\log(Ni^{2+})$ scale for the NiO domain is obtained by plotting Eq. (8a); it is noteworthy that the properties of the system depend only on pCO_2 and not on the redox potential. This is the case until the oxygen pressure is reduced to the dissociation pressure of NiO ($10^{-19.16}$ atm) when nickel metal may again appear. Thus the line on the diagram for $\log(O_2) = -19.16$ is the boundary between the NiO and Ni domains.

APPLICATION OF THE DIAGRAMS

General

In general a corroding metal will not be in equilibrium with the melt, and some assumption must be made to enable the use of these diagrams.. For aqueous systems Pourbaix[5] made the arbitrary assumption that a metal would corrode if the equilibrium concentration of its ions were greater than 10^{-6}M; if less, the metal was said to be immune. This should be useful as a rough guideline in treating the molten carbonate system. It is assumed that the metal satisfies the Temkin[16] model for the liquid state. This permits the thermodynamic activities to be replaced by

concentrations in units of mole fraction.

The use of the diagrams may be illustrated by considering the behavior of nickel at 600°C (Fig. 2). If nickel metal is immersed in the carbonate melt under an atmosphere of carbon dioxide, the 'normal operating conditions' might be 0.9 atmos. CO_2 and 0.1 atmos. O_2. This would approximate to the point on the diagram $pCO_2 = 0$, $E = 0$. This is in the region of oxide-cover, and the concentration of Ni^{2+} ions in the melt is as low as $10^{-5}M$. Two possibilities exist: either the metal will corrode completely to oxide; or the NiO will form a coherent film on the metal surface and lead to passivation. The thermodynamic treatment cannot distinguish these two possibilities and experimental data are required. However, the treatment indicates that oxide formation is inevitable unless the CO_2 pressure is increased to 10^{5} atmos. or the O_2 pressure reduced to 10^{-19} atmos. It seems that the only sure way of preventing attack on nickel lies in cathodic protection; reduction of the potential to -0.8V should remove any oxide and render the metal immune.

Comparison of Metals

Iron (Fig. 3). For simplicity only the ferrous oxidation state has been considered. The striking feature of the diagram is the general

similarity to that of nickel. Even though the standard potential of iron (-0.66V) is somewhat lower than for nickel (-0.34V), under 'normal operating conditions' the system is in the FeO domain, and the concentration of Fe^{2+} is 10^{-5}M. Once again one sees there is a possibility of passivation if the oxide forms a coherent film.

Silver (Fig. 4). Under 'normal operating conditions' silver oxide is unstable and there is now no chance of spontaneous passivation. The metal is in equilibrium with Ag^{+} ions at a concentration 10^{-3}M, and it seems certain that the metal will corrode.

Gold (Fig. 5). For gold also the oxide is unstable under the usual conditions, but the equilibrium concentration of Au^{3+} ions is less than 10^{-10} M. One should expect gold to be completely immune from attack either to form oxide or to dissolve in the melt.

Platinum (Fig. 6). An interesting feature is that point E = 0, pCO_2 = 0 lies just beneath (50mV) the boundary line for the PtO and Pt domains. The metal should be in equilibrium with its ions at 10^{-6} M and therefore be immune. However, if an oxide phase should form, the solubility of Pt^{2+} will be as low as 10^{-5}M and passivity will be a possibility.

All these metals described above have been investigated by potentiostatic and other techniques[1,2,3,4] and their corrosion behavior is well established. The comparison between thermodynamic predictions and experiment is shown in Table 1. Within the limitation of the thermodynamic method, there is good agreement.

DISCUSSION

The success of the treatment in accounting for the behavior of five metals suggests its essential validity. Its extension to a wide range of metals might give an insight into the general electrochemistry of the molten carbonate system. Table 2 summarizes the data for a number of metals considered. The first column E^{o}, is the electrochemical series in molten carbonates, the parallelism with its aqueous analogue being quite striking. It has been found that only gold and platinum are sufficiently 'noble' to be immune from attack, and so protection of other metals will depend either on cathodic protection or on passivation.

The second column, $E(10^{-6}M)$, contains the potentials required to give really effective cathodic protection. It is apparent that with metals more active than iron, complications may arise from the decomposition of the melt or the deposition of graphite.

Inspection of the third column reveals that the oxides of all the metals from nickel upwards are stable at this temperature, and hence the important factor must be the solubility of the oxide in the melt. The final column contains the pCO_2 values at which the oxide will precipitate from the molten metal carbonate. The metals may be divided into two categories. In the first group are the alkali metals and barium; these do not precipitate except at large positive values of pCO_2, and hence give rise to good carbonate solvents. The second class comprises the remaining metals, where it is apparent that oxide precipitation occurs even at significantly negative values of pCO_2, i.e. under more acid conditions than are generally encountered. This frequent formation of insoluble oxide gives good reason to believe that a systematic study of passivation behavior will be worthwhile.

The importance of pCO_2 in corrosion phenomena indicates that acid-base considerations will be helpful in understanding the behavior of refractory oxides. Thus, the dissolution of magnesia in the melt will be governed by the equilibrium:

$$\underset{\text{(base)}}{MgO} + \underset{\text{(acid)}}{CO_2} \rightleftharpoons \underset{\substack{\text{(conjugate)}\\ \text{acid}}}{Mg^{2+}} + \underset{\substack{\text{(conjugate)}\\ \text{base}}}{CO_3^{=}}$$

and $$K_b = \frac{(Mg^{2+})(CO_3^{=})}{(MgO)(CO_2)} \qquad (9)$$

If excess MgO is present at unit activity, log $K_b = pCO_2$ when $(Mg^{2+}) = 1$. Thus the pCO_2 values in Table 2 are the log K_b values for the basic oxides in the molten carbonate solvent. Magnesia has been shown[1] to have excellent properties as a container material and it seems that other less basic oxides could be equally suitable.

The corresponding behavior of acidic oxides is interesting in this context. If the interaction of silica with the melt is represented as:

$$\underset{\text{(acid)}}{SiO_2} + \underset{\text{(base)}}{Na_2CO_3} \rightleftharpoons \underset{\substack{\text{(conjugate)}\\ \text{base}}}{Na_2SiO_3} + \underset{\substack{\text{(conjugate)}\\ \text{acid}}}{CO_2}$$

then
$$K_a = \frac{(SiO_3^{=})(CO_2)}{(CO_3^{=})(SiO_2)} \qquad (10)$$

If SiO_2 is present at unit activity, pKa = pCO_2 when $(SiO_3^{=}) = (CO_3^{=})$. The pKa value may thus be understood as the value of pCO_2 when the contamination of the melt is reversed. Thus, when $pCO_2 = pK-1$, $(SiO_3^{=}) = 0.09$, and when $pCO_2 = pK+1$, $(SiO_3^{=}) = 0.91$. Calculated values for silica and alumina are: $pKa_{SiO_2} = -2.46$; $pKa_{Al_2O_3} = +1.37$. This is in accord with the observation that silica glass rapidly dissolves in carbonate melts while porcelain reference electrodes[17] are attacked only slowly. In this way it is possible to relate the position of all acid-base equilibria within the melt

to the pressure of carbon dioxide, and the usefulness of pCO_2 as an acidity function is seen.

It is not suggested that the E-pCO_2 diagrams provide a complete description of the interaction between metal substrates and fused carbonate systems. The thermodynamic approach can cast no light on the structural and kinetic features which are so often important. It is suggested that the merit of the treatment lies in the correlation of substrate reactivity with acid base behavior, giving a better perspective of the corrosion phenomena.

ACKNOWLEDGEMENT

This work was made possible in large part by financial support received from the U. S. Department of Navy, Office of Naval Research, Chemistry Division Washington, D.C.

REFERENCES

1. G.J. Janz, A. Conte and E. Neuenschwander, Corrosion, 19,292t (1963).
2. G.J. Janz and A. Conte, ibid 20,238t (1964).
3. G.J. Janz and A. Conte, Electrochimica Acta, (in press).
4. G.J. Janz and A. Conte, ibid (in press).
5. M. Pourbaix, "Thermodynamics of Dilute Aqueous Solutions", Arnold, London (1949).
6. R. Littlewood, J. Electrochem. Soc., 109, 525 (1962).

7. H. Lux, Z. Elektrochem., 45, 303 (1939).

8. H. Flood and T. Forland, Acta Chem. Scand., 1, 592 (1947).

9. K.K. Kelley and C. T. Anderson, U.S.Bur. Mines, Bull. 384 (1935).

10. C.E. Wicks and F. E. Block, ibid Bull. 605 (1963).

11. JANAF Thermochemical Tables, Advanced Research Projects Agency Program, U.S.Air Force Contract No. AF 33(616)-6149.

12. O. Kubaschewski and E.L. Evans, "Metallurgical Thermochemistry" Pergamon Press, London (1958).

13. H. Flood, T. Forland and K. Motzfelt, Acta Chem. Scand., 6,257 (1952).

14. G.K. Stepanow and A.M. Trunow, Dokl. Akad. Nauk S.S.S.R.,142,886 (1962).

15. G.H.J. Broers, Ph.D. Thesis, Amsterdam (1958).

16. M. Temkin, Acta Physicochim. U.R.S.S., 20, 411 (1945).

17. P. Degobert and O. Bloch, Bull. Soc. Chim. (France), 13, 1887 (1962).

TABLE CAPTIONS

Table 1 'Corrosion Behavior of Selected Metals in the Ternary Eutectic at 600°C.'

Table 2 'Summary of Electrochemical Data in Molten Carbonates at 600°C.'

FIGURE CAPTIONS

Figure 1 'E -pCO_2 Diagram showing Redox and Acid Base Equilibria in the Ternary Eutectic at 600°C.'

Figure 2 'E-pCO_2 Diagram for the system Nickel-Ternary Eutectic at 600°C.'

Figure 3 'E-pCO_2 Diagram for the system Iron-Ternary Eutectic at 600°C.'

Figure 4 'E-pCO_2 Diagram for the system Silver-Ternary Eutectic at 600°C.'

Figure 5 'E-pCO_2 Diagram for the system Gold-Ternary Eutectic at 600°C.'

Figure 6 'E-pCO_2 Diagram for the system Platinum-Ternary Eutectic at 600°C.'

Table 1

Corrosion Behavior of Selected Metals

In the Ternary Eutectic at 600°C

Metal	Theoretical 'Domain'	Experimental[1,2,3,4]
Au	immune	no corrosion, no oxide
Pt	immune or oxide-cover	passive
Ag	corrosion	corrodes to Ag^+
Fe (stainless steel)	oxide-cover	passive
Ni	oxide-cover	corrodes to Ni O

Table 2

Summary of Electrochemical Data In Molten Carbonates at 600°C

Metal	Electrode Potential		Oxide Pressure	Oxide Precipitation
	E^o	$E(10^{-6}M)$	log (O_2)	p CO_2
Ba	-2.90V	-3.42V	-56.86	+5.50
Li	-2.87	-3.91	-54.90	+6.09
Ca	-2.59	-3.11	-65.20	-2.27
K	-2.45	-3.49	-27.34	+15.0
Na	-2.43	-3.47	-35.1	+10.9
Mg	-2.41	-2.93	-50.80	-2.18
Mn	-1.38	-1.90	-38.42	-2.88
Zn	-0.89	-1.41	-31.02	-4.79
Fe (II)	-0.66	-1.18	-24.70	-4.34
Co	-0.39	-0.91	-20.88	-5.52
Ni	-0.34	-0.86	-19.16	-5.24
Pt	(+0.52)	0.00	+0.28	(-5.24)
Ag	+0.55	-0.49	+2.48	-4.50
Au	(+0.84)	+0.49	+9.4	(-4.50)

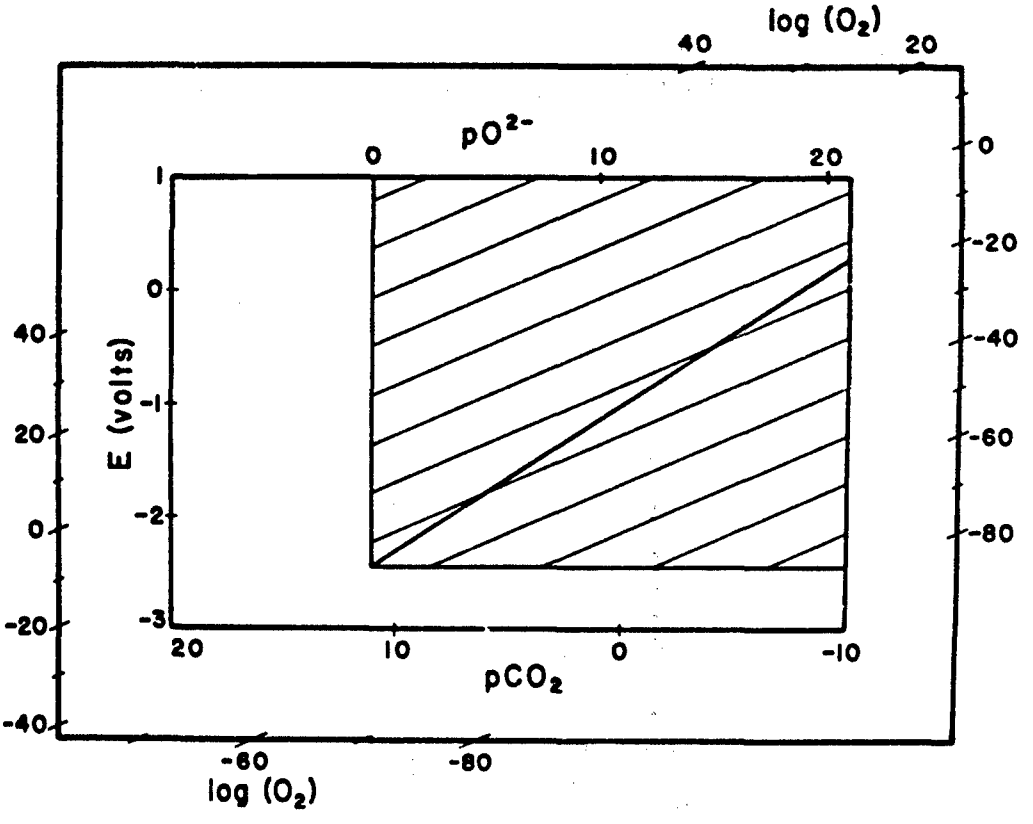
log (O2)
40
20
pO2-
0
10
20
1
0
-1
-2
-3
E (volts)
40
20
0
-20
-40
20
10
0
-10
pCO2
0
-20
-40
-60
-80
log (O2)

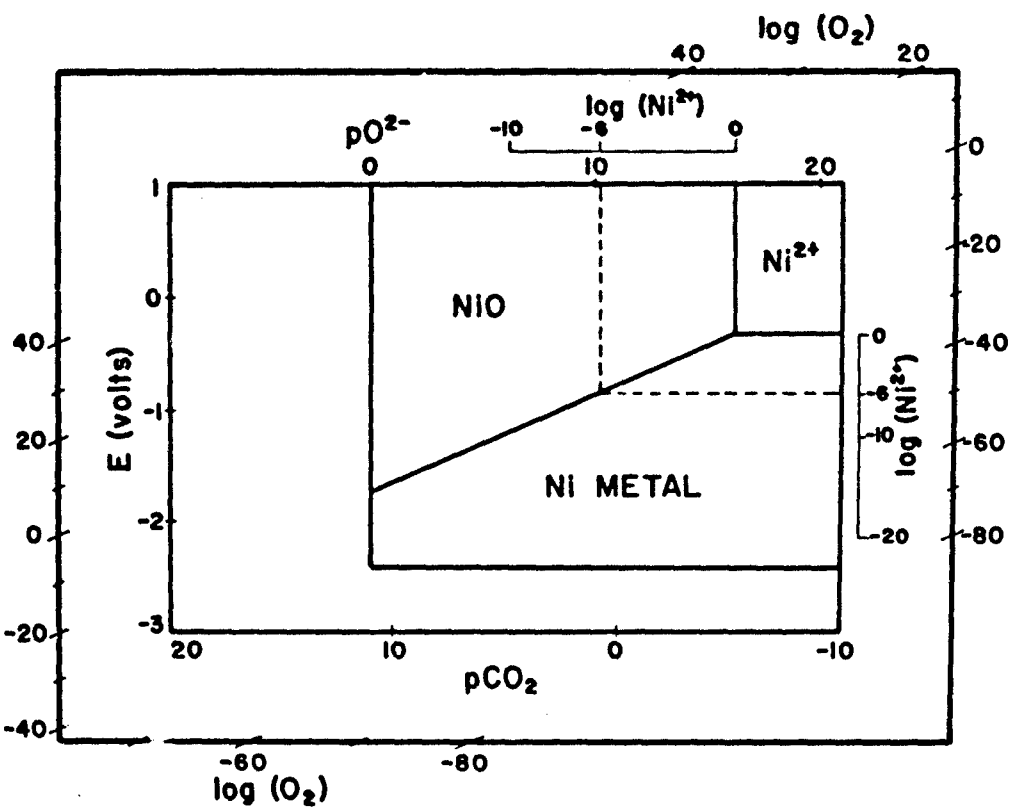
log (O2)
40
20
pO2-
log (Ni2+)
-10
-6
0
0
10
20
1
0
-1
-2
-3
NiO
Ni2+
Ni METAL
E (volts)
40
20
0
-20
-40
0
-6
-10
-20
log (Ni2+)
0
-20
-40
-60
-80
20
10
0
-10
pCO2
-60
-80
log (O2)

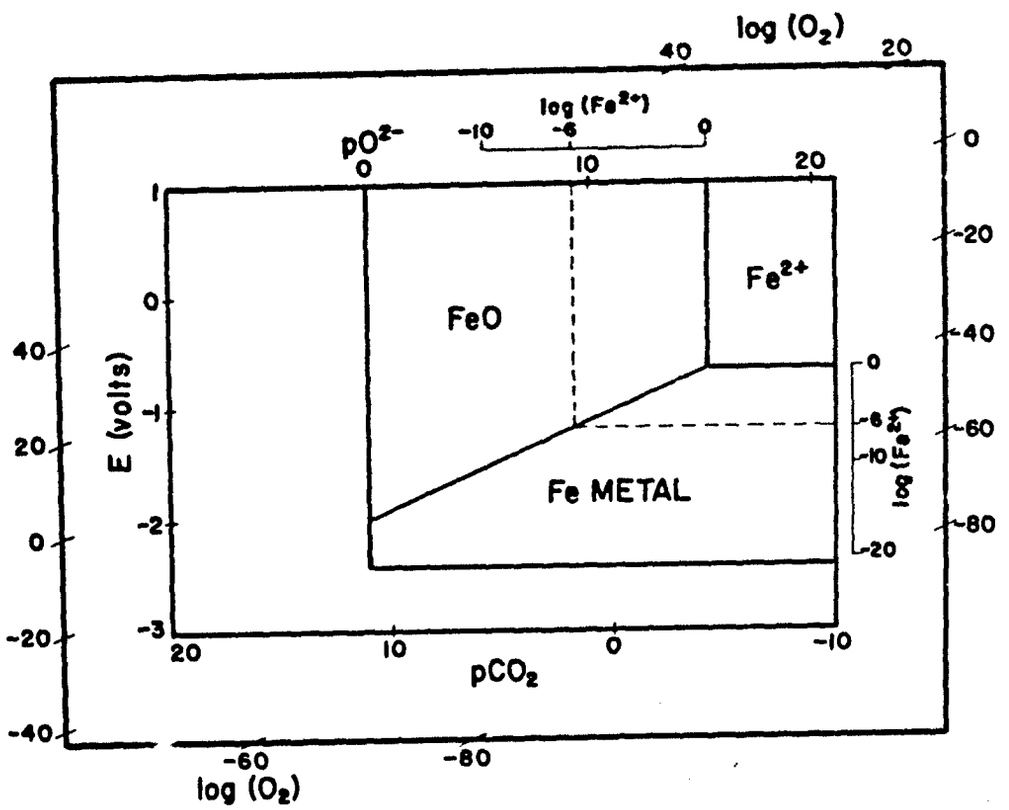
log (O2)
40
20
log (Fe2+)
-10
-6
0
pO2-
0
10
20
1
0
-1
-2
-3
FeO
Fe2+
Fe METAL
E (volts)
40
20
0
-20
-40
0
-20
-40
-60
-80
0
-6
-10
-20
log (Fe2+)
20
10
0
-10
pCO2
-60
-80
log (O2)

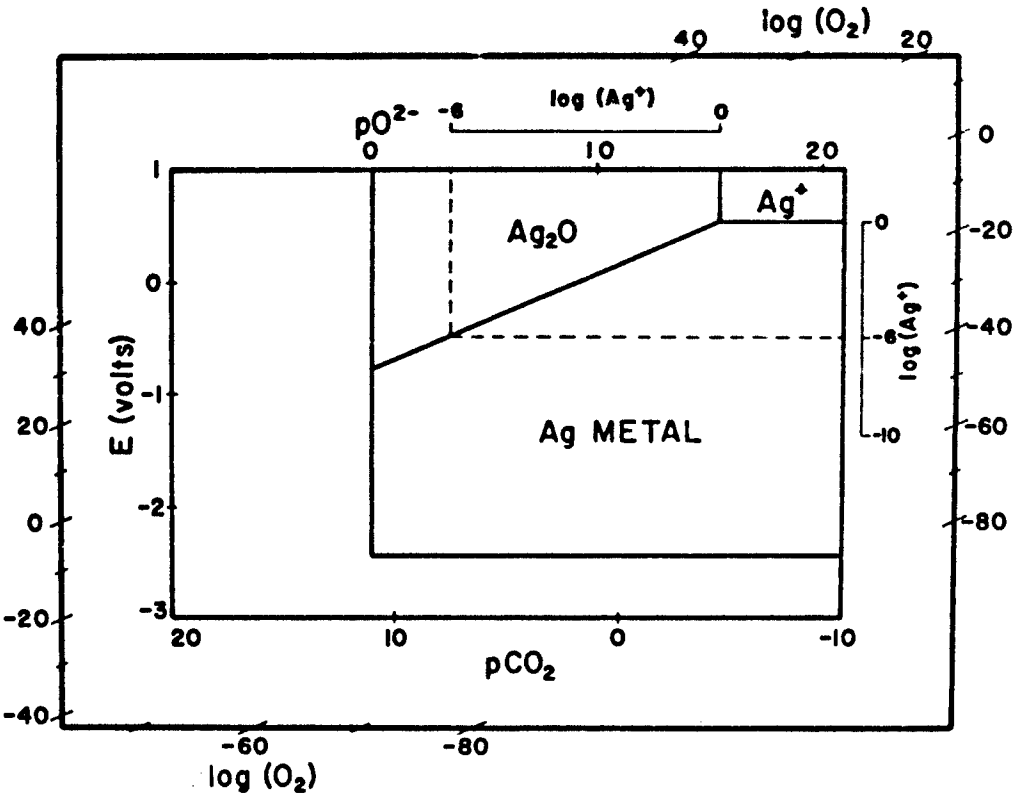
log (O2)
40
20
pO2-
-6
log (Ag+)
0
0
10
20
1
0
-1
-2
-3
E (volts)
Ag2O
Ag+
Ag METAL
0
-6
-10
log (Ag+)
0
-20
-40
-60
-80
40
20
0
-20
-40
20
10
0
-10
pCO2
-60
-80
log (O2)

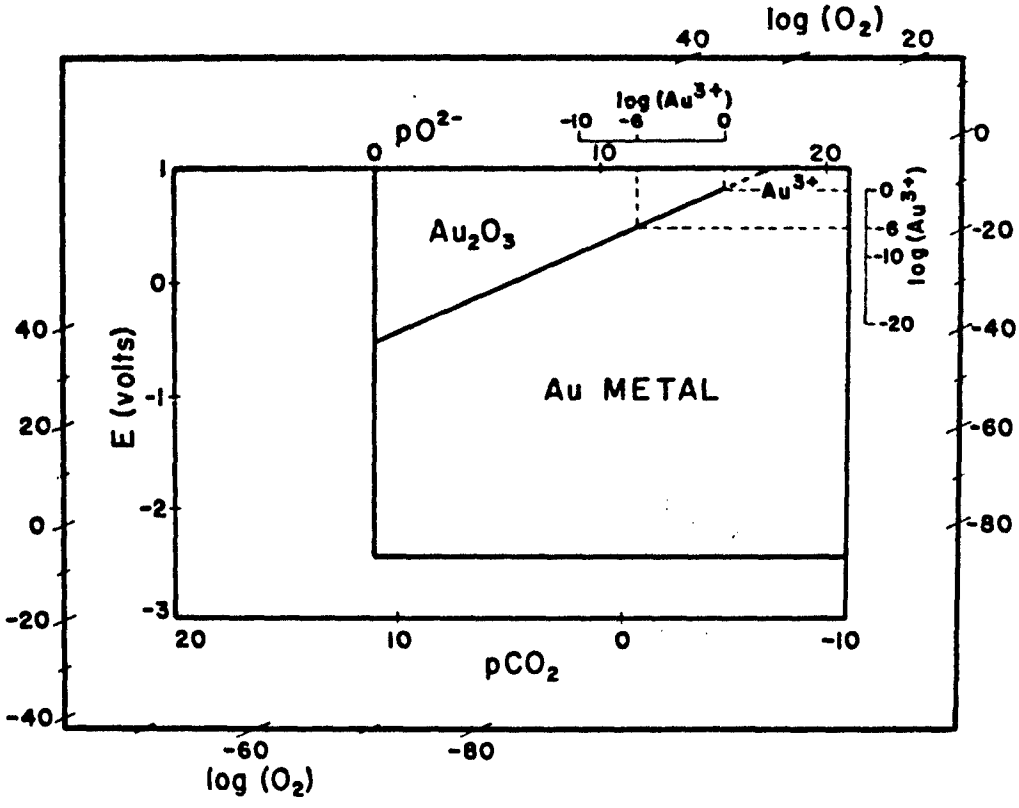
log (O2)
40
20
log (Au3+)
-10 -6 0
pO2-
0
10
20
0
Au3+
Au2O3
0 -6 -10 -20
log (Au3+)
1
0
-1
-2
-3
E (volts)
40
20
0
-20
-40
-20
-40
-60
-80
Au METAL
20
10
0
-10
pCO2
-60
-80
log (O2)

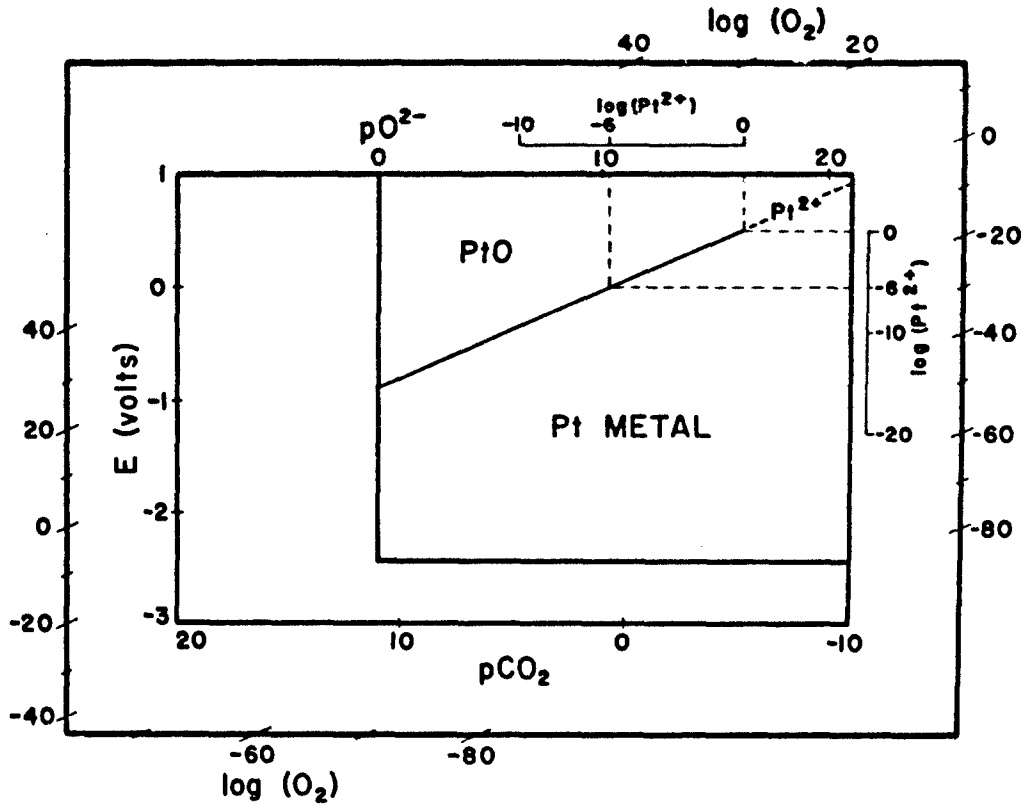
log (O2)
40
20
pO2-
0
log(Pt2+)
-10
-6
0
10
20
1
0
-1
-2
-3
PtO
Pt2+
Pt METAL
0
-6
-10
-20
log (Pt2+)
E (volts)
40
20
0
-20
-40
-60
-80
20
10
0
-10
pCO2
log (O2)

TECHNICAL REPORT DISTRIBUTION LIST

Commanding Officer
Office of Naval Research Branch Office
230 N. Michigan Avenue
Chicago 1, Illinois (1)

Commanding Officer
Office of Naval Research Branch Office
207 West 24th Street
New York 11, New York (1)

Commanding Officer
Office of Naval Research Branch Office
1030 East Green Street
Pasadena 1, California (1)

Commanding Officer
Office of Naval Research Branch Office
Box 39, Navy 100, F.P.O.
New York, N.Y. (7)

Director, Naval Research Laboratory
Washington 25, D.C.
Attn: Technical Information Officer (6)
Chemistry Division (2)
Code 6160 (1)

Chief of Naval Research
Department of the Navy
Washington 25, D.C.
Attn: Code 425 (2)

DDR and E
Technical Library
Room 3C-128, The Pentagon
Washington 25, D.C. (1)

Department of the Army
Supply and Maintenance Command
Maintenance Readiness Division
Washington 25, D.C.
Attn: Technical Director (1)

U.S. Army Natick Laboratories
Clothing and Organic Materials Division
Natick, Massachusetts
Attn: Associate Directory (1)

Harry Diamond Laboratories
Washington 25, D.C.
Attn: Library (1)

Office, Chief of Research and Development
Department of the Army
Washington 25, D.C.
Attn: Physical Sciences Division (1)

Chief, Bureau of Ships
Department of the Navy
Washington 25, D.C.
Attn: Code 342A (2)

Technical Library Library, DLI-3
Bureau of Naval Weapons
Department of the Navy
Washington 25, D.C. (4)

Defense Documentation Center
Cameron Station
Alexandria, Virginia (20)

Commanding Officer
U.S. Army Electronics Research and
Development Laboratory
Attn: SELRA/DR
Fort Monmouth, New Jersey 07703 (1)

Naval Radiological Defense Laboratory
San Francisco 24, California
Attn: Head, Chemistry Division (1)

REVISED 30 AUG 1963

Technical Report Distribution List

Commanding Officer
Army Research Office
Box CM, Duke Station
Durham, North Carolina
Attn: CRD-AA-IP (1)

Atomic Energy Commission
Division of Research
Chemistry Programs
Washington 25, D.C. (1)

Atomic Energy Commission
Division of Technical Information Ext.
Post Office Box 62
Oak Ridge, Tennessee (1)

Commanding Officer
U.S. Army Chemical Research and
Development Laboratories
Attn: Librarian (1)
Edgewood Arsenal, Maryland

Dr. Norman Hackerman
Department of Chemistry
University of Texas
Austin, Texas (1)

Dr. Paul Delahay
Department of Chemistry
Louisiana State University
Baton Rouge, Louisiana (1)

Dr. J. O'M Bockris
Department of Chemistry
University of Pennsylvania
Philadelphia, Pennsylvania (1)

Dr. R.R. Heikes
Solid State Phenomena Department
Westinghouse Electric Corporation
Pittsburgh, Pennsylvania (1)

Dr. Ernest Yeager
Department of Chemistry
Western Reserve University
Cleveland 6, Ohio (1)

Dr. Pierre van Rysselberghe
Deparment of Chemistry
Stanford University
Palo Alto, California (1)

Dr. A. Patterson, Jr.
Department of Chemistry
Yale University
New Haven, Connecticut (1)

Mr. M.F. Blackburn
E.R.D.L.
Materials Branch
Fort Belvoir, Virginia (1)

Mr. W.M. Lee, Director
Contract Research Department
Pennsalt Chemicals Corporation
900 First Avenue
King of Prussia, Pa. (2)

Dr. B.R. Sundheim
Department of Chemistry
New York University
New York 3, New York (1)

Commanding Officer
U.S. Naval Ordnance Laboratory
Corona, California
Attn: Library (1)

Dr. Morris Eisenberg
Electrochimica Corporation
307 Diablo Court
Palo Alto, California (1)

U.S. Naval Applied Science Laboratory
Technical Library
Building 291, Code 9832
Naval Base
Brooklyn, N.Y. 11251 (1)

E.C. Wadlow
Department of Material Research
Queen Anne Mansions
St. James Park
London, S.W. 1
VIA: Commanding Officer
Office of Naval Research Branch Office
Navy 100 Box 39, F.P.O.
New York, N.Y. (1)

Monsanto Research Corporation
Everett Station
Boston 49, Massachusetts
Attn: Library (1)

Dr. E.M. Cohn
NASA
Code RPP
1512 H. Street, N.W.
Washington 25, D.C. (1)

Dr. M.S. Cohen, Chief
Propellants Synthesis Section
Reaction Motors Division
Denville, New Jersey (1)

Dr. Paul W. Gilles
Department of Chemistry
The University of Kansas
Lawrence, Kansas (1)

Dr. William T. Biedler
Research Laboratories
United Air Corp.
Silver Lane
East Hartford, 8, Conn. (1)

Dr. A.C. Makrides
Tyco, Inc.
Bear Hill
Waltham, Massachusetts (1)

Dr. G.C. Szego
Institute for Defense Analysis
1666 Connecticut Avenue, N.W.
Washington 9, D.C. (1)

Dr. S.P. Wolsky, Director
Laboratory for Physical Science
P.R. Mallory, Inc.
N.W. Industrial Park
Burlington, Mass. (1)

Dr. A.B. Scott
Department of Chemistry
Oregon State University
Corvallis, Or.

Dr. Isaac Trachtenberg
Energy Research Laboratory
Texas Instruments Inc.
Research Building
13500 North Central Expressway
Dallas, Texas (1)

Aerospace Corporation
P.O. Box 95085
Los Angeles 45, California
Attn: Library Technical Documents
Group (1)